Electronic Supplementary Material (ESI) for Inorganic Chemistry Frontiers.

Electronic Supplementary Materials

Boosting Photochemical Activity by Ni Doping of Mesoporous CoO Nanoparticle Assemblies

Georgia Velegraki,[a] Ioannis Vamvasakis,[a] Ioannis T. Papadas,[b] Sotiris Tsatsos,[c] Anastasia Pournara,[d] Manolis J. Manos,[d] Stelios A. Choulis,[b] Stella Kennou,[c] Georgios Kopidakis,[a] Gerasimos S. Armatas*[a]

[a] *Department of Materials Science and Technology, University of Crete, Heraklion 71003, Greece.*
[b] *Department of Mechanical Engineering and Materials Science and Engineering, Cyprus University of Technology, Limassol 3041, Cyprus.*
[c] *Department of Chemical Engineering, University of Patras, Patra 26504, Greece.*
[d] *Department of Chemistry, University of Ioannina, Ioannina 45110, Greece.*

*E-mail: garmatas@materials.uoc.gr

Supporting Tables

Table S1. Electrochemical properties of mesoporous $Co_{1-x}Ni_xO$ MNAs catalysts (pH 7).

Sample	Energy gap (E_g) (eV)	E_{FB} (V vs NHE)	E_{CB} (V vs NHE)	Carrier density (N_A, cm^{-3})
CoO MNAs	2.50	1.15	-1.35	3.31×10^{16}
$Co_{0.99}Ni_{0.01}O$ MNAs	2.63	1.17	-1.46	3.98×10^{16}
$Co_{0.98}Ni_{0.02}O$ MNAs	2.66	1.20	-1.46	3.82×10^{16}
$Co_{0.95}Ni_{0.05}O$ MNAs	2.69	1.22	-1.47	4.57×10^{16}

Table S2. EIS equivalent circuit fitted parameters of pure and Ni-doped CoO MNAs catalysts.

Sample	R_s (Ω)	Q_f (F)	L_{ad} (H)	R_{ct} (Ω)	Q_{dl} (F)	x^2
CoO MNAs	2.94	10.41×10^{-9}	74.04×10^{-6}	103.8	42.70×10^{-6}	1.5×10^{-3}
$Co_{0.99}Ni_{0.01}O$ MNAs	3.05	10.77×10^{-9}	73.20×10^{-6}	100.7	51.78×10^{-6}	2.3×10^{-3}
$Co_{0.92}Ni_{0.02}O$ MNAs	3.18	10.76×10^{-9}	73.55×10^{-6}	100.5	39.82×10^{-6}	3.4×10^{-3}
$Co_{0.95}Ni_{0.05}O$ MNAs	3.08	10.82×10^{-9}	73.53×10^{-6}	99.8	36.00×10^{-6}	3.6×10^{-3}

Supporting Figures

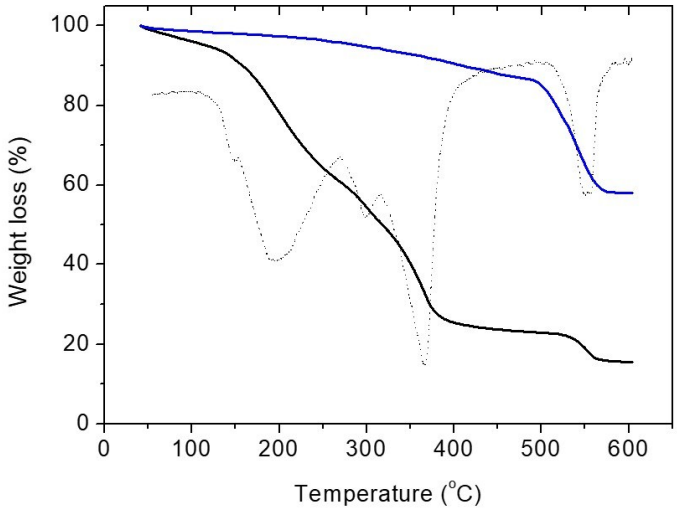

Fig. S1 TGA profiles of (a) as-prepared containing surfactant (black line) and (b) mesoporous CoO MNAs recorded under N_2 flow (~200 mL min^{-1}). The differential thermogravimetric (DTG) curve (dotted line) for as-prepared material is also given.

The TGA plot of mesostructured CoO material shows a weight loss of ~5.2% in the 40–120 °C temperature range due to the removal of residual solvent and a 71.9% weight loss between 120 and 500 °C, which is attributed to the decomposition of organic polymer. The weight loss (~7.4%) observed in the temperature range 500–600 °C is attributed to the reduction of CoO to Co. The TGA plot of mesoporous CoO MNAs sample shows a ~2.5% weight loss between 40 and 180 °C due to the removal of physisorbed solvents and a weight loss of ~10.6% in the 180–480 °C temperature range, which is attributed to the decomposition of residual carbon species. The weight loss of ~28.7% observed between 480 and 600 °C is attributed to the reduction of CoO to Co (Fig. S2).

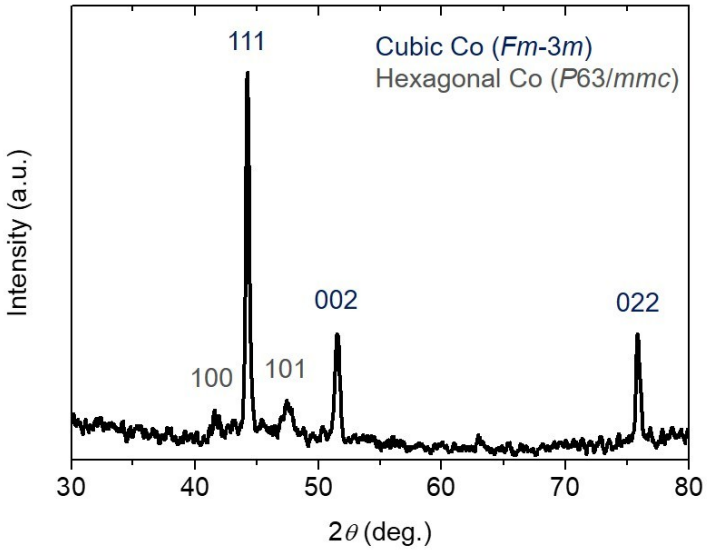

Fig. S2 XRD pattern of the inorganic residue obtained after TGA analysis of the CoO mesoporous sample (up to 600 °C, in N_2). All diffraction peaks could be indexed to the metallic Co with a face-centered cubic (JCPDS No. 15-0806) and hexagonal close-packed (JCPDS No. 05-0727) structure.

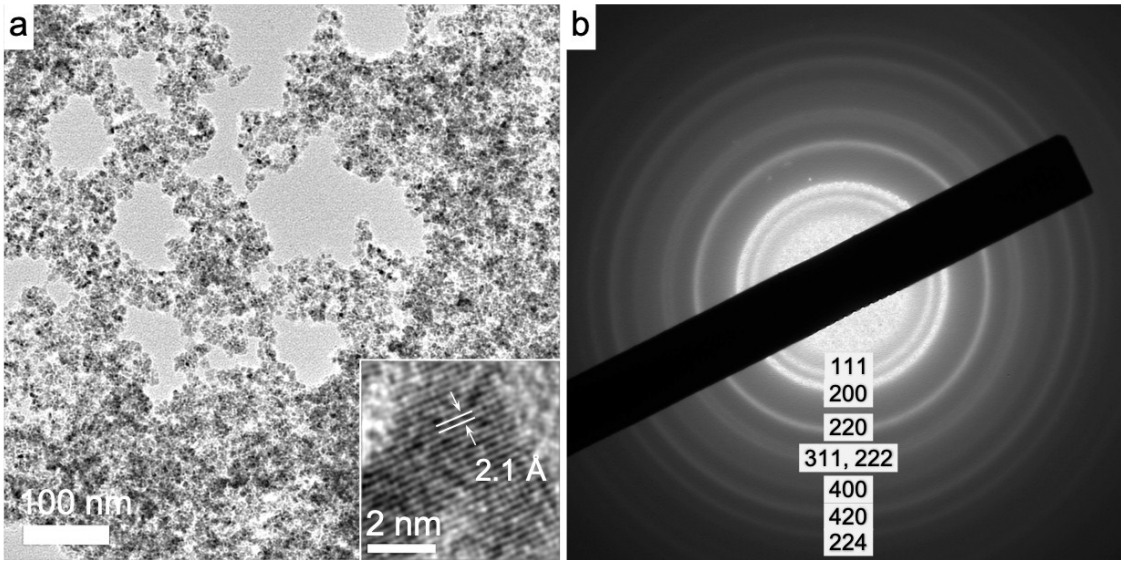

Fig. S3 (a) Typical TEM images and (b) SAED pattern of CoO MNAs.

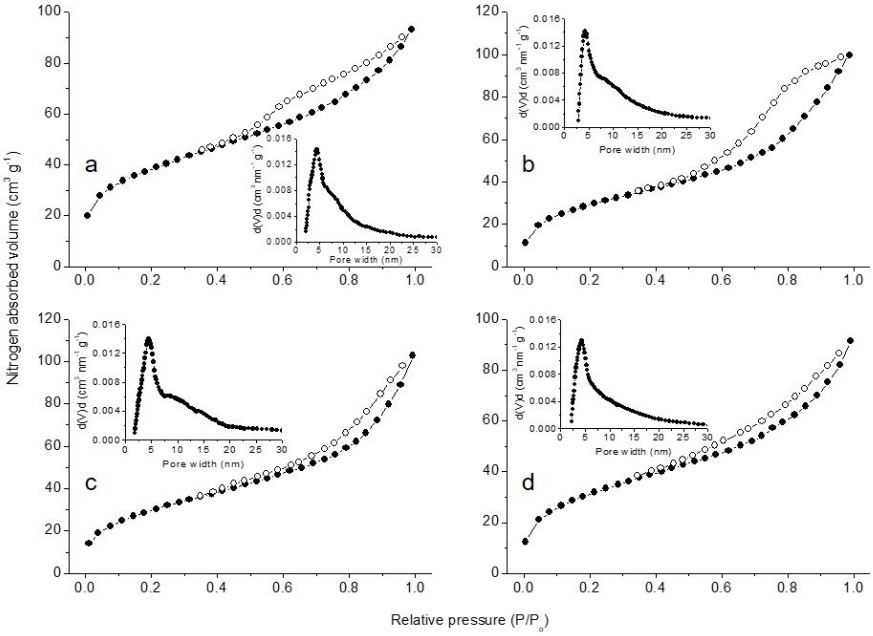

Fig. S4 N_2 adsorption (filled cycles) and desorption (open cycles) isotherms at –196 °C and the corresponding NLDFT pore-size distribution (insets) for $Co_{1-x}Ni_xO$ MNAs: (a) x = 0, (b) x = 0.01, (c) x = 0.02 and (d) x = 0.05. All the materials showed type-IV adsorption-desorption isotherms with a H_3 type hysteresis loop, which is characteristic of mesoporous solids with slit-like pores.

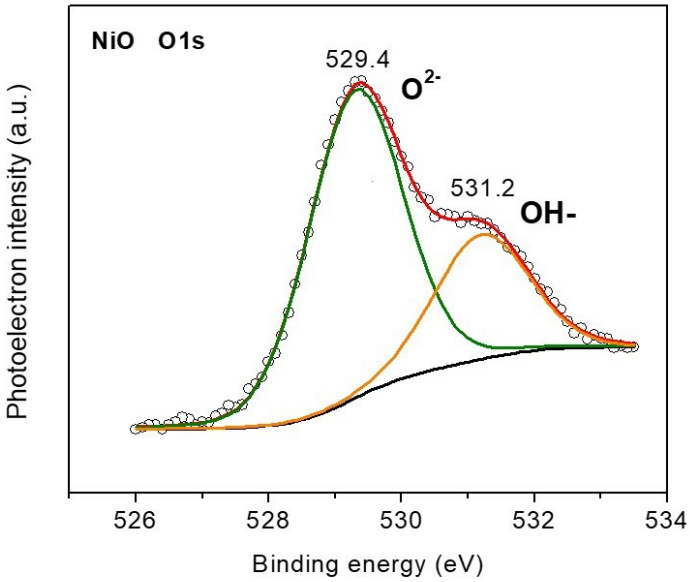

Fig. S5 O 1s XPS spectrum of the polycrystalline NiO material.

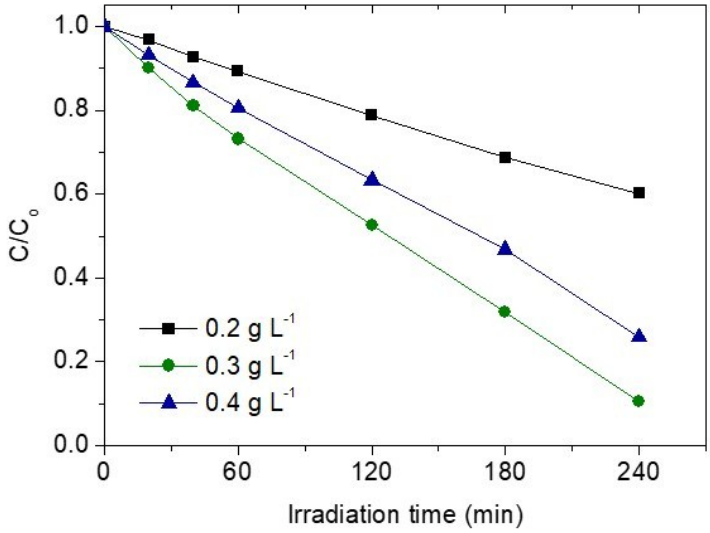

Fig. S6 Concentration dependent photocatalytic Cr(VI) reduction activity of $Co_{0.98}Ni_{0.02}O$ MNAs. Reaction conditions: 0.2–0.4 g L^{-1} of catalyst, 50 mg L^{-1} Cr(VI) aqueous solution, pH = 2, UV-visible light (λ > 360 nm) irradiation, 20 ^{o}C.

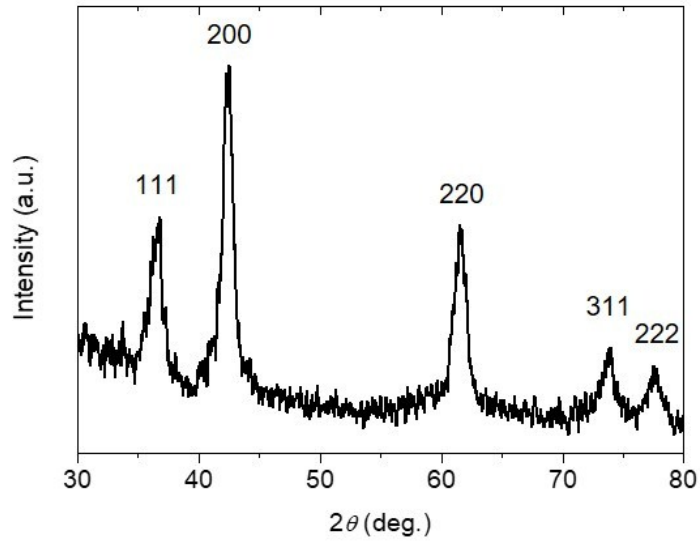

Fig. S7 Powder XRD pattern of the reused $Co_{0.98}Ni_{0.02}O$ MNAs catalyst. All the diffraction peaks in the XRD pattern can be assigned to the cubic phase of CoO (JCPDS No. 43-1004).

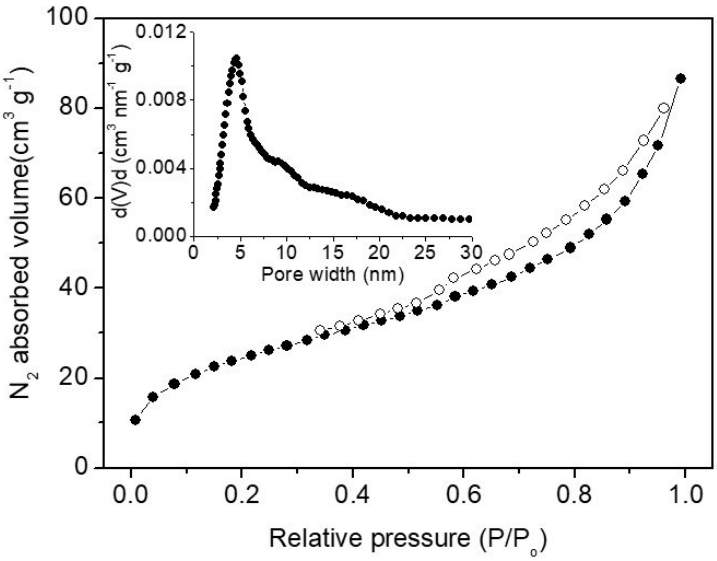

Fig. S8 N_2 adsorption-desorption isotherms at –196 °C (Inset: the corresponding NLDFT pore-size distribution, indicating an average pore size of ~4.6 nm) of the $Co_{0.98}Ni_{0.02}O$ MNAs catalyst retrieved after the cycling test. Analysis of the adsorption data indicate a BET surface area of 92 m^2g^{-1} and a pore volume of 0.13 cm^3g^{-1}.

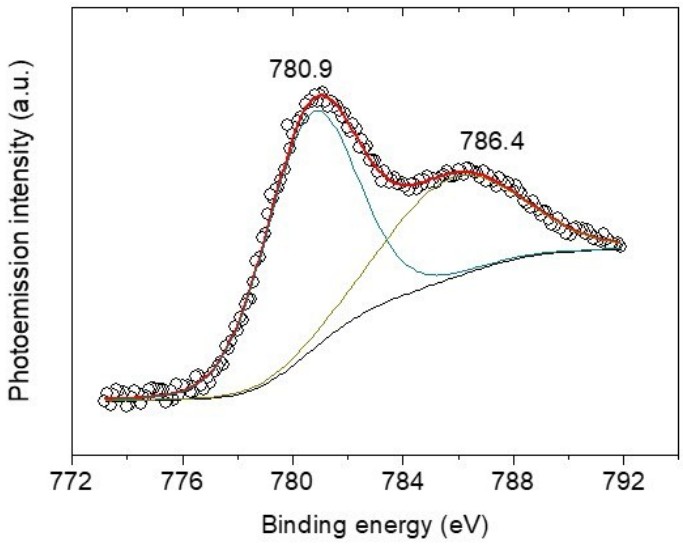

Fig. S9 Co $2p_{3/2}$ XPS spectrum of the $Co_{0.98}Ni_{0.02}O$ MNAs catalyst obtained after catalysis, showing a Co $2p_{3/2}$ peak at 780.9 eV associated with a shake-up satellite peak at 786.4 eV.

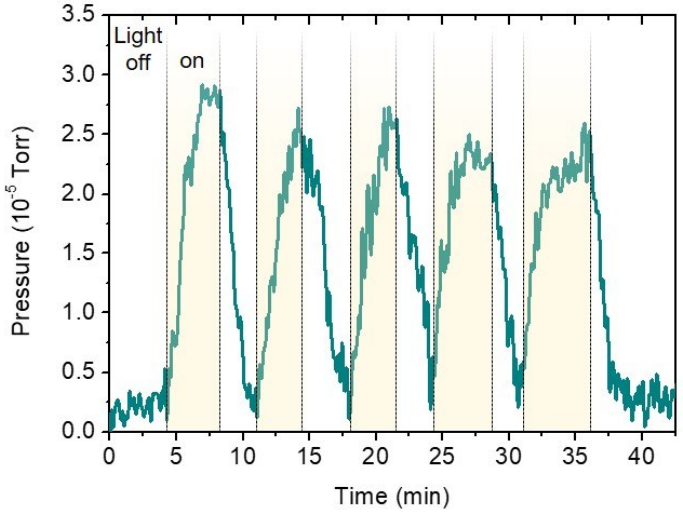

Fig. S10 O_2 evolution transient with light on/off for $Co_{0.98}Ni_{0.02}O$ MNAs catalyst under λ > 360 nm light irradiation.

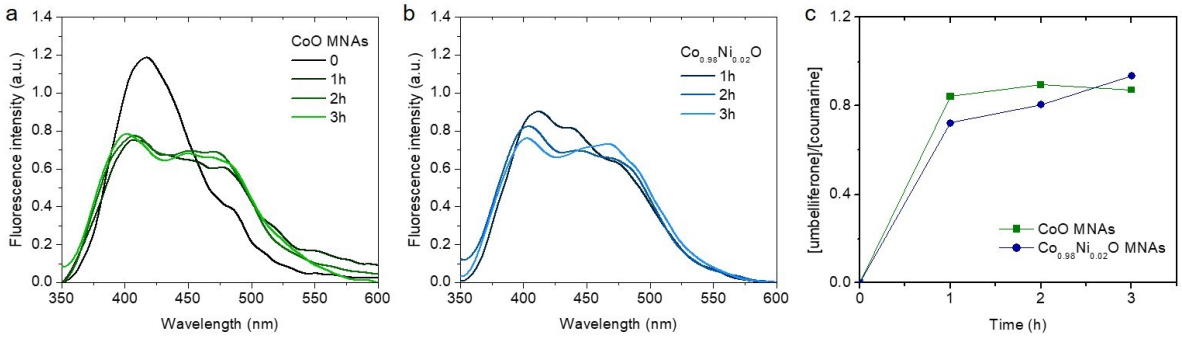

Fig. S11 (a, b) Fluorescence spectra of coumarin in water and (c) time evolution of the fluorescence intensity ratio of umbelliferone emission (455 nm) to coumarine emission (398 nm) for CoO and $Co_{0.98}Ni_{0.02}O$ MNAs catalysts. The emission peaks at ~398 nm and ~455 nm correspond to the coumarin and umbelliferone, respectively. All the •OH radical formation tests were performed similarly to the photocatalytic Cr(VI) reduction reactions, but with the addition of coumarin in the solution. Reaction conditions: 0.3 g L^{-1} catalyst, 10 mM coumarin, 50 mg L^{-1} Cr (VI) solution, pH = 2, UV–vis light (λ > 360 nm) irradiation, 20 °C. Fluorescence emission spectra obtained with an excitation wavelength of 332 nm.

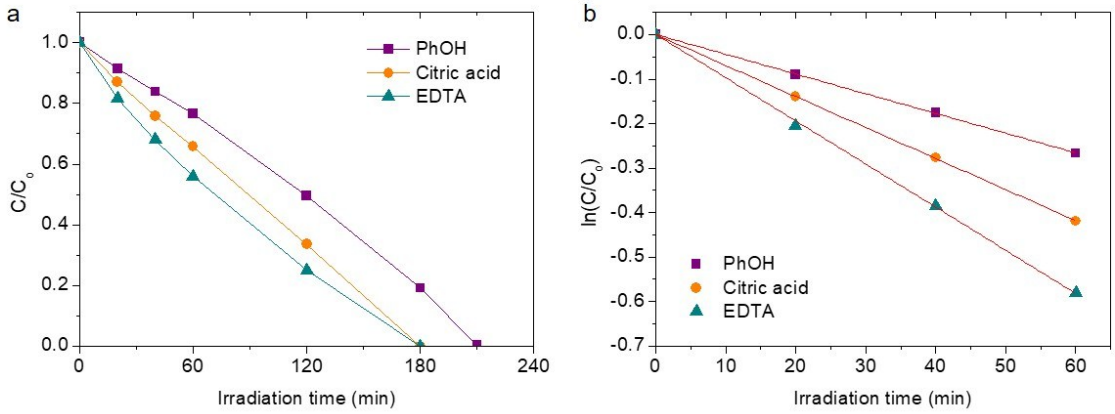

Fig. S12 (a) Photocatalytic reduction of aqueous Cr(VI) and (b) kinetic profiles over $Co_{0.98}Ni_{0.02}O$ MNAs catalyst in the presence 1 equiv. of phenol, citric acid or EDTA under λ > 360 nm light irradiation. Reaction conditions: 0.3 g L^{-1} catalyst, 50 mg L^{-1} Cr(VI) solution, pH = 2, 20 °C. In panel (b), the red lines are fit to the data.